# Superdense core mode in the Large Helical Device with an internal diffusion barrier[a)]

T. Morisaki,[b)] N. Ohyabu, S. Masuzaki, M. Kobayashi, R. Sakamoto, J. Miyazawa, H. Funaba, K. Ida, K. Ikeda, O. Kaneko, S. Morita, S. Mutoh, K. Nagaoka, Y. Nagayama, N. Nakajima, K. Narihara, Y. Oka, M. Osakabe, B. J. Peterson, S. Sakakibara, M. Shoji, Y. Suzuki, Y. Takeiri, N. Tamura, K. Tanaka, K. Tsumori, K. Y. Watanabe, I. Yamada, H. Yamada, A. Komori, O. Motojima, and LHD Experiment Group
*National Institute for Fusion Science, Toki 509-5292 Japan*

(Received 11 June 2006; accepted 26 February 2007; published online 2 May 2007)

In reduced recycling discharges using a local island divertor in the Large Helical Device [O. Motojima, H. Yamada, A. Komori *et al.*, Phys. Plasmas **6**, 1843 (1999)], a stable high-density plasma develops in the core region when a series of pellets is injected. A core region with $\sim 5 \times 10^{20}$ m$^{-3}$ and temperature of 0.85 keV is maintained by an internal diffusion barrier (IDB). The density gradient at the IDB ($r/a \sim 0.6$) is very high, and the particle confinement time in the core region is $\sim$0.4 s. Because of the increase in the central pressure, a large Shafranov shift up to $\sim$0.3 m is observed. The critical ingredients for IDB formation are a strongly pumped divertor to reduce edge recycling, and multiple pellet injection to ensure efficient central fueling. No serious magnetohydrodynamics activity and impurity accumulation have been observed so far in this improved discharge. © *2007 American Institute of Physics*. [DOI: 10.1063/1.2718530]

## I. INTRODUCTION

To achieve a burning plasma is the final goal for the toroidal magnetic confinement fusion research.[1] Much effort and time have been paid to discover a breakthrough toward this goal. Various confinement improved modes, i.e., H-mode,[2] internal transport barriers (ITBs),[3–5] and so on, have been discovered mainly in tokamaks. For the helical device,[6] which is an alternative approach aiming at the same goal, the discovery of the improved modes for particle and energy confinement is also an urgent issue to be solved.

In the Large Helical Device (LHD) project,[7] one of the most important research goals is to realize a reactor-relevant plasma through effective edge control with divertors. Two completely different divertor configurations are employed in LHD: the helical divertor (HD)[8] and the local island divertor (LID).[9–12] The HD is an intrinsic helical double-null divertor that is similar to the tokamak double-null divertor except for its long connection length of the field lines in the thick ergodic region surrounding the closed surfaces.[13] On the other hand, the LID is an alternative divertor concept of the HD with outstanding capability of edge plasma control.[11,12] Although the present HD is an open configuration (without baffles and active pumping), the LID has a fully closed configuration with strong pumping capability.

Recently, a superdense core (SDC) mode,[12,14] consequently achieved with the formation of an internal diffusion barrier (IDB), was discovered on the LHD in the LID configuration with a central fueled condition by the repetitive pellet injection.[15] In this mode, a superdense plasma with the central density of $\sim 5 \times 10^{20}$ m$^{-3}$ is maintained by the formation of an IDB with extremely high-density gradient. Although use of the LID reduces the confinement volume by $\sim$40% from the nominal value, IDB-SDC modes exhibit the highest performance ($n_0 T_0 \tau_E = 4.4 \times 10^{19}$ m$^{-3}$ keV s) obtained so far in the LHD.[14]

Similar high-density improved modes have been observed in tokamaks and stellarators. The pellet enhanced performance (PEP) mode[16] was achieved in the Joint European Torus.[17] In the PEP mode, central deposition from pellet fueling and central heating in the ion cyclotron range of frequencies can lead to strongly peaked density profiles that produce the ITBs with the negative shear region in the plasma core.[18,19] In the Wendelstein stellarator (W7-AS),[20] another improved confinement mode called the high-density H-mode (HDH) was achieved, which is characterized by flat density profiles and low impurity confinement time.[21,22] In the HDH, impurity contamination is avoided, which is also seen in the IDB-SDC mode in the LHD [see Sec. III D].

In this paper, the characteristics of the IDB-SDC mode are mainly described, together with its future aiming at the reactor plasma. After describing a short introduction to the LID and experimental setup, together with experimental conditions in Sec. II, experimental results are shown in Sec. III. Before summarizing in Sec. V, some discussions aiming at the reactor plasma are described in Sec. IV.

## II. EXPERIMENTAL APPARATUS AND CONDITIONS

The LHD is the largest superconducting heliotron device, with poloidal/toroidal period numbers of 2/10, major radius and averaged plasma minor radius of 3.5–4.1 m and 0.6 m, respectively, and toroidal magnetic field of 3.0 T.[7] The Thomson scattering system provides the electron density $n_e$ and temperature $T_e$ profiles. The line averaged density is measured with a far-infrared interferometer. Total radiation power from impurities is measured with a bolometer array

[a)]Paper NI1 1, Bull. Am. Phys. Soc. **51**, 176 (2006).
[b)]Invited speaker. Electronic mail: morisaki@nifs.ac.jp

 

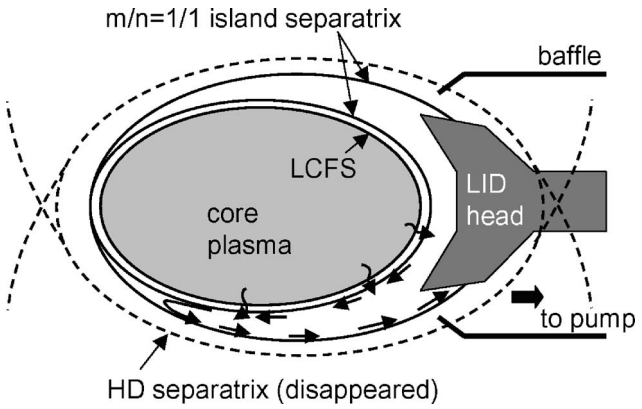


FIG. 1. A schematic of the LID.

and line emissions from impurities are also measured with spectroscopic method. Especially for metallic impurities (e.g., Fe, Cr, Ti), a pulse height analyzer (PHA) for the x-ray range emission is utilized. Plasma stored energy is measured with a diamagnetic loop.

The LID is a kind of island divertor.[11,21–24] A schematic of the LID is presented in Fig. 1. An externally induced $m/n=1/1$ island located in the edge region is utilized by LID, where $m$ and $n$ are poloidal and toroidal mode numbers, respectively. Particles diffusing out from the core region cross the island separatrix and flow along the periphery of the island. After several toroidal turns, they reach the outer separatrix of the island where the LID head is placed, and strike its backside on which they are neutralized. Particles recycled there are pumped out efficiently by the strong pumping system with a baffle integrated into the closed divertor configuration. In the LID configuration, the boundary of the confinement region is defined with the inner island separatrix. Field lines in or near the island are cut by the LID head, thus removing all closed flux surfaces and ergodic region there.

In the experiment, the IDB-SDC mode was produced in the LID configuration with strong edge-pumping capability. The magnetic axis position $R_{ax}$ was set at 3.75 m, which is relatively an outward shifted configuration from the standard one, i.e., $R_{ax}=3.60$ m, where the LHD has its best confinement performance.[25] Three neutral beams (NBs) with a total heating power of ~10 MW were injected to heat and sustain the plasma. Repetitive pellet injectors were utilized to realize the central fueling.

## III. EXPERIMENTAL RESULTS

### A. Typical IDB-SDC mode

As mentioned in Sec. I, the IDB-SDC mode is obtained in the LID configuration when a series of pellets are injected. These pellets penetrate beyond the magnetic axis and bring about the central deposition of the fueling particles. The time evolutions of some principle parameters are presented in Fig. 2. The density profile in the initial phase is flat and low. After several pellets of $\Delta n \sim (2-3)\times 10^{21}$ are injected to the NB heated plasma, the density profile takes on a peaked shape, which can be seen from the abrupt rise in central density $n_{e0}$

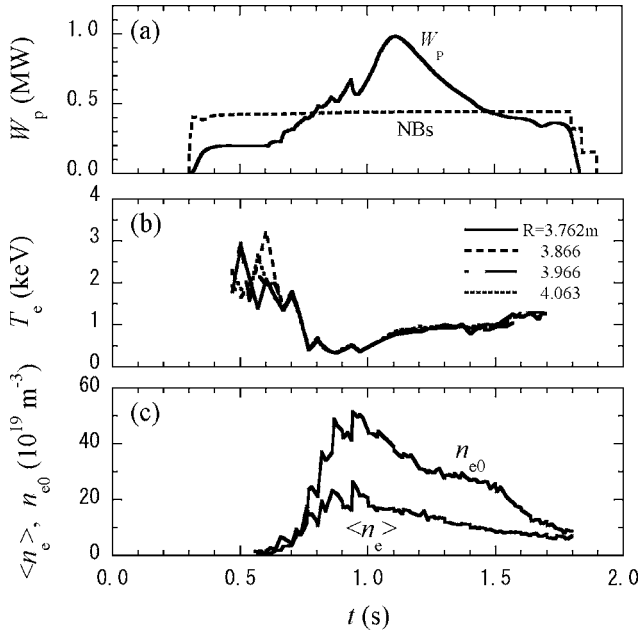


FIG. 2. Time evolutions of (a) stored energy $W_p$ together with the injection sequence of NBs, (b) electron temperature $T_e$ in the core region, and (c) central electron density $n_{e0}$ and averaged density $\langle n_e \rangle$ in the typical IDB-SDC mode.

and its separation from the averaged density $\langle n_e \rangle$ at $t \sim 0.76$ s, as shown in Fig. 2(c). Subsequent pellet injection continuously raises $n_{e0}$ until the final pellet is injected at $t \sim 0.95$ s. Since the NBs are still heating the plasma, electron temperature $T_e$ at the central region starts to rise [Fig. 2(b)], according to the decrease of the electron density, as shown in Fig. 2(c). In this phase, no gas puff is injected. The plasma stored energy $W_p$ keeps on rising until $t=1.1$ s because the relative increase in temperature is larger than the simultaneous decrease in density.

The typical radial electron density and temperature profiles at the time when $W_p$ reaches its maximum are depicted in Fig. 3. A core region with electron density ~$5\times 10^{20}$ m$^{-3}$ and temperature ~0.85 keV is maintained by an IDB, which provides the highest fusion plasma performance, i.e., $n_0 T_0 \tau_E \sim 4.4\times 10^{19}$ keV m$^{-3}$ s,[14] achieved so far on

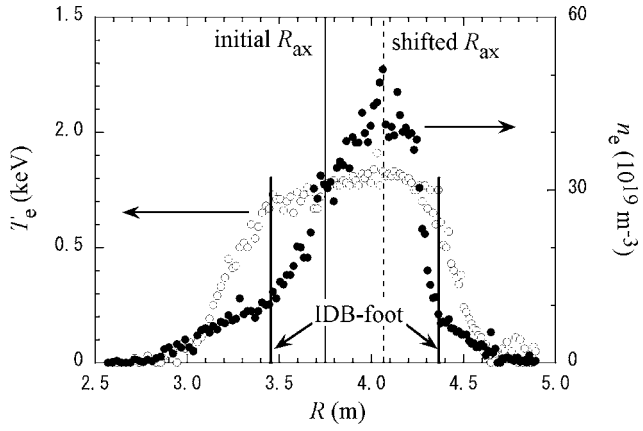


FIG. 3. Typical electron density (closed circles) and temperature (open circles) profiles in the IDB-SDC mode.

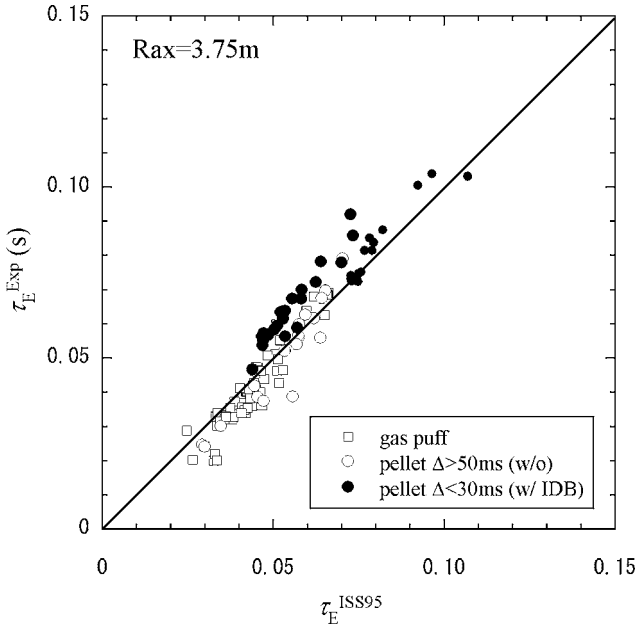


FIG. 4. Comparison of energy confinement time $\tau_E$ between experimental result and expectation by ISS95 scaling law.

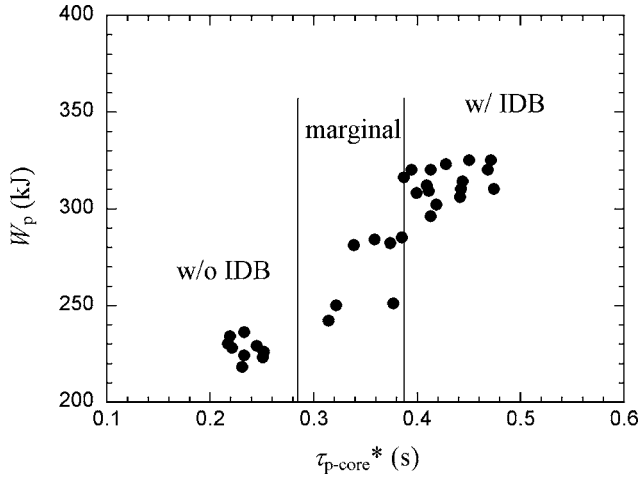


FIG. 5. Relationship between stored energy $W_p$ and the effective particle confinement time $\tau^*_{\text{p-core}}$ inside the IDB.

LHD. The extremely steep density gradient is formed on the IDB foot, which is depicted with thick solid line(s) in Fig. 3, while the temperature gradient is not so steep there. Outside the IDB, the density gradient is moderate. The radial width of the IDB is about 0.1 (outboard side of the torus) −0.4 (inboard side) m. Due to the high central pressure, a large Shafranov shift of ~0.3 m is observed. The original magnetic axis position and the shifted one are depicted with a thin solid line and a dashed line, respectively, in the figure. In this discharge, the central beta value $\beta_0$ is 4.4%. In the LHD, the typical $\beta_0$ equivalent to this discharge without an IDB is less than 2%.

### B. Global confinement

In order to investigate the effect of the IDB on global confinement, the energy confinement time $\tau_E$ was derived and its improvement from the ISS95 scaling law[26] was estimated. Figure 4 shows the result of comparisons among three different samples: gas puff shots, pellet shots without the IDB, and pellet shots with the IDB. We have never seen the IDB-SDC mode in discharges fueled with gas puff. Even with the pellet discharges, the repetitive pellet injection with its injection period longer than 50 ms cannot form the IDB.[12] In this figure, therefore, pellet discharges with injection period shorter than 30 ms achieved the IDB-SDC mode (closed circles). It can be seen that gas puff shots and pellet shots without the IDB almost follow the ISS95 scaling law. On the other hand, $\tau_E$ with the IDB is higher than that expected with the scaling. The $\tau_E$ itself is longer than other discharges without the IDB. In ordinary discharges in the HD configuration (without IDB), the confinement performance generally degrades with the increase of density.[27] However, the IDB formation improves the energy confinement up to 20% from ISS95 scaling law.

The formation of the steep density gradient in the IDB-SDC mode is considered to be attributed to the improvement of particle confinement. It is generally difficult to estimate the particle confinement time in non-steady-state discharges. In this study, we estimated the effective particle confinement time inside the IDB by measuring the density decay time after the pellet injection. Results are shown in Fig. 5. The $\tau^*_{\text{p-core}}$ in the figure is the effective particle confinement time inside the IDB, derived from the time constant of the density decay measured with the center chord of the interferometer. Note that this experiment was done with relatively low heating power (~2.8 MW), in other words, with relatively low central density, in order to avoid fringe jumps in interferometer signals. For this reason, achieved $W_p$ is not so high. However, the IDB formation was confirmed in these discharges with proper experimental conditions; e.g., the time interval of the repetitive pellet injection. In Fig. 5, the IDB is not observed in discharges with $\tau^*_{\text{p-core}} < 0.26$ s; on the other hand, discharges with $\tau^*_{\text{p-core}} > 0.38$ s have an IDB and relatively high central density. It is found that the plasma stored energy $W_p$ increases with $\tau^*_{\text{p-core}}$ and the discharges with an IDB have long $\tau^*_{\text{p-core}}$. In Fig. 5, circles $0.3 < \tau^*_{\text{p-core}} < 0.38$ are from the marginal phase. This is due to the characteristics of the IDB formation, i.e., which is not accompanied by a fast and/or clear transition phenomenon.

### C. Magnetohydrodynamic (MHD) activities

Since the IDB-SDC mode has quite a steep density gradient and consequent pressure gradient in the confinement region, its equilibrium and stability are a matter of great concern. Numerical analyses using the three-dimensional equilibrium code VMEC[28] and the ideal MHD stability analysis code CAS3D[29] were performed. Pressure profiles used in analyses are depicted in Fig. 6(a). The solid line is an experimentally measured pressure profile where $\langle\beta\rangle = 1.4\%$ and $\beta_0 = 4.4\%$, and dotted and dashed lines are profiles in which enhanced pressure is assumed in the calculations. In the dashed line case, pressure increases from the foot point of the IDB; on the other hand, the whole region is enhanced in

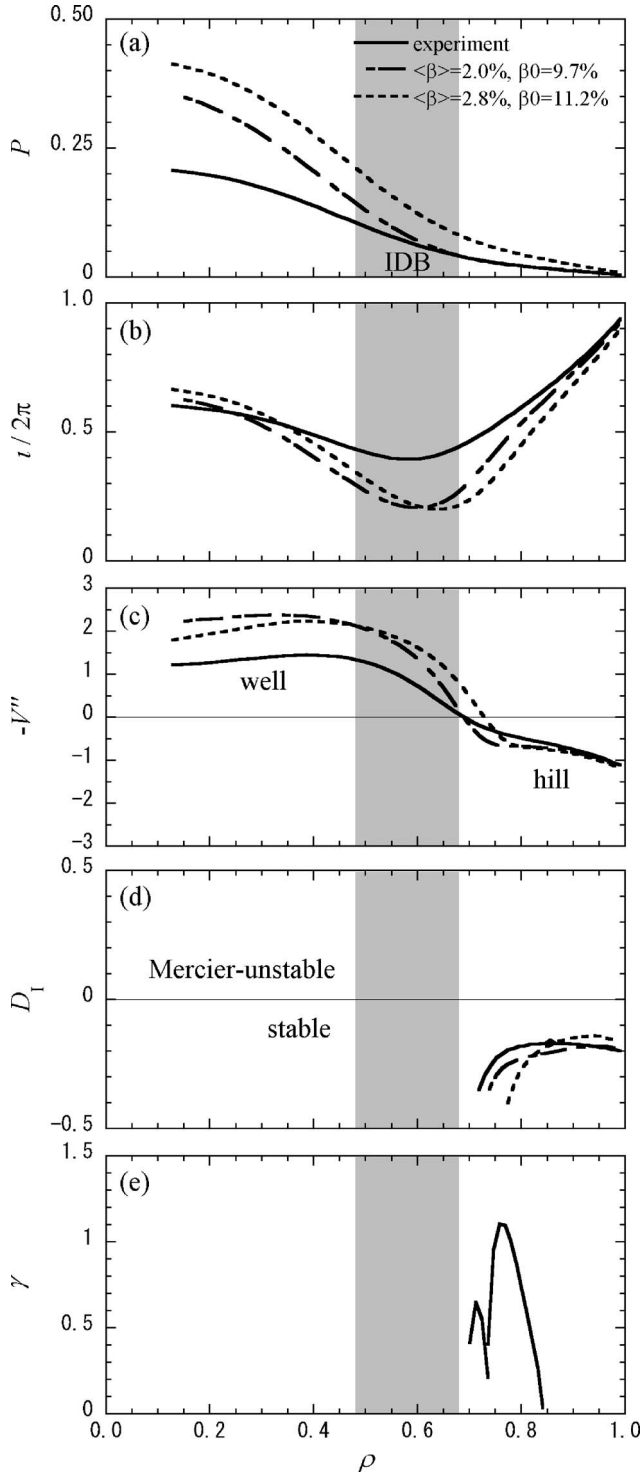


FIG. 6. Radial profiles of (a) pressure $P$, (b) normalized rotational transform $\iota/2\pi$, (c) magnetic well and hill $V''$, (d) Mercier criterion $D_I$, and (e) growth rate of the ideal ballooning mode $\gamma$.

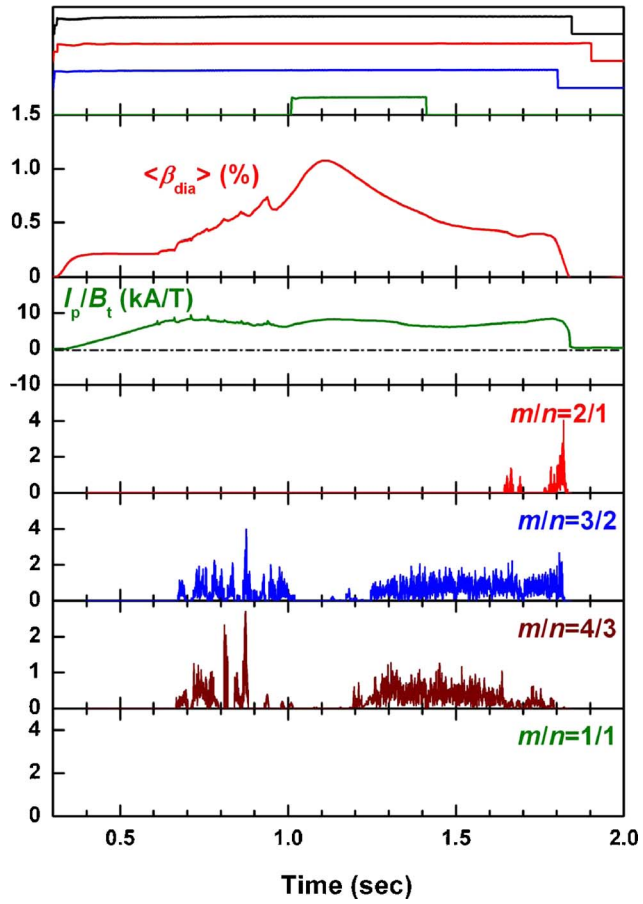


FIG. 7. (Color online) From top to bottom: NB injection sequence, time evolutions of volume averaged beta value $\langle\beta_{\rm dia}\rangle$, plasma current $I_p$ normalized by toroidal magnetic field $B_t$, and Mirnov coil signals.

the dotted line case. It can be seen, from the normalized rotational transform profile $\iota/2\pi$ in Fig. 6(b), that the magnetic shear reverses around the IDB, even at $\langle\beta\rangle=1.4\%$ in the experiment. Due to the large Shafranov shift, a large magnetic well region spreads out beyond the IDB, as shown in Fig. 6(c), and the $D_I$ is quite low, which means Mercier stable, in the whole region [Fig. 6(d)]. The analysis by the CAS3D code indicates that ideal ballooning modes are also stable in the whole region in the discharge obtained in the experiment, as known from Fig. 6(e), showing its growth rate to be negative (not drawn). The core region inside the IDB is stable against the ideal interchange mode, even in the higher beta regime up to $\langle\beta\rangle\sim1.4\%$ and $\beta_0\sim10\%$, which is much higher than that achieved in the experiment so far. However, as far as the ideal ballooning mode is concerned, its growth rate appears to be positive in such a high beta regime in the edge region, as shown in Fig. 6(e). The core region inside the IDB is still stable against the ballooning mode.

During the IDB-SDC mode, MHD activities were experimentally measured with Mirnov coil arrays installed in poloidal and toroidal directions in the vacuum vessel of the LHD. Figure 7 shows the Mirnov coil signals together with the NB injection sequence (top), volume averaged beta value $\langle\beta_{\rm dia}\rangle$, and plasma current $I_p$ normalized by toroidal magnetic field $B_t$. Magnetic fluctuations whose poloidal/toroidal mode numbers $m/n=3/2$ and $4/3$ are observed. These modes are excited in the outer region of the IDB, as shown in Fig. 8, which describes $\iota/2\pi$ profile at $\langle\beta\rangle=0.66\%$ and $1.20\%$, calculated with the VMEC code. The normalized pressure profile $P/P_0$ and the IDB position are also depicted in the figure. No unstable mode inside the IDB is observed. The $m/n=3/2$ and $4/3$ modes disappear during $1\ {\rm s}<t<1.2\ {\rm s}$ when the

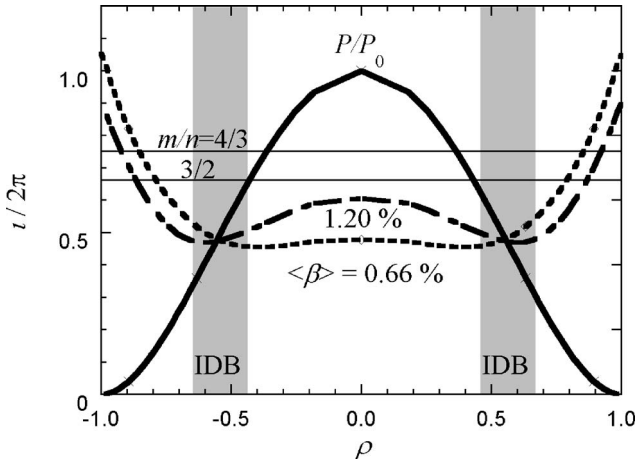


FIG. 8. Radial profiles of the normalized rotational transform $\iota/2\pi$ at $\langle\beta\rangle$ =0.66% and 1.20% calculated with the VMEC code, and normalized pressure $P/P_0$ used in the calculation. IDB positions are also depicted in the figure.

beta value is around its maximum. In such a high beta regime, rational surfaces related to $m/n=3/2$ and $4/3$ modes are pushed out of the confinement region where the LID head cuts the magnetic field lines. That is the reason these modes disappear in the high beta regime during the discharge. After the beta value decreases in the latter half of the discharge, those modes appear again. Concerning the fluctuation amplitude of these modes, they are too small to disturb or destroy the IDB. These experimental results described above agree well with the calculation results.

Another experimental result also supports the VMEC/CAS3D expectations. The relationship between $\langle\beta_{\mathrm{dia}}\rangle$ and the pressure gradient was examined. Figure 9 shows the dependence of edge (open circles) and core (closed circles) gradients on $\langle\beta_{\mathrm{dia}}\rangle$. The core gradient means the IDB gradient. It is clearly seen that both gradients increase with $\langle\beta_{\mathrm{dia}}\rangle$. The core gradient is higher than that of the edge even in the low beta regime, which may simply be attributed to the particle source. In the low beta regime, the IDB is weak or not perfectly formed yet; however, the particle source is in the core region due to pellet injection, which may be the reason for

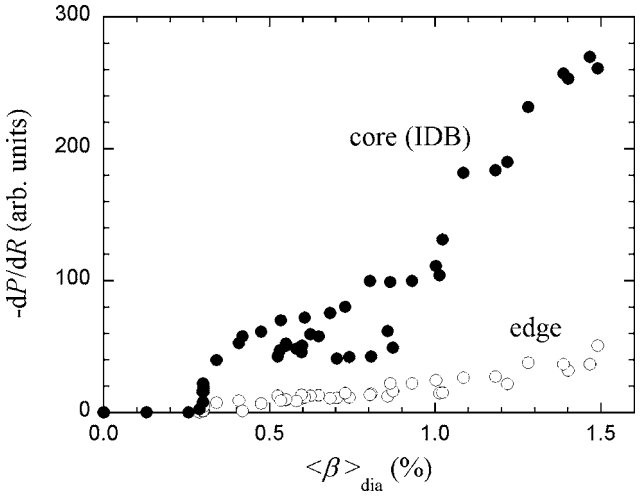


FIG. 9. Relationship between core and edge gradients and beta.

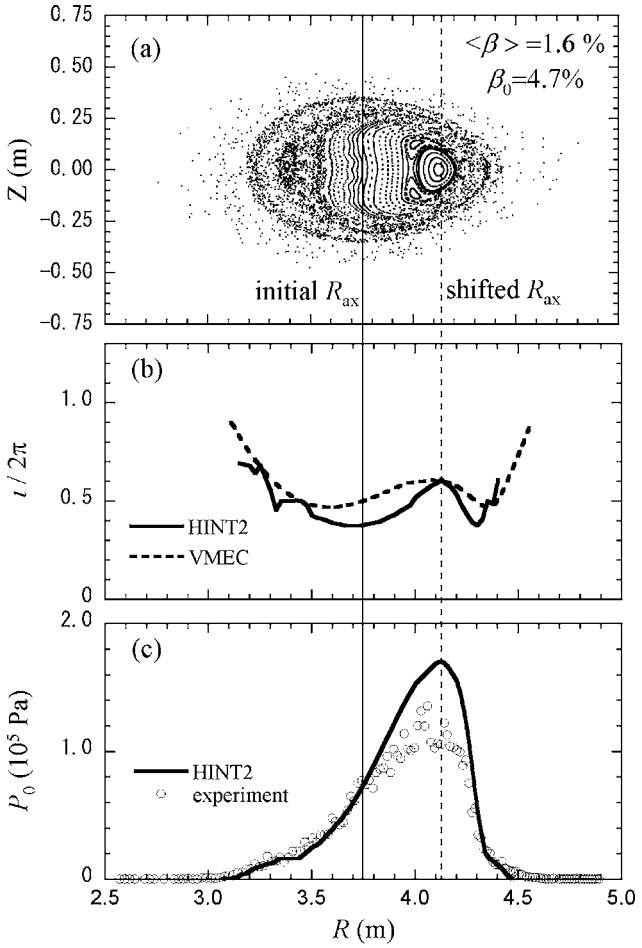


FIG. 10. Results of the HINT2 code. (a) Poincaré plot of the magnetic surfaces, (b) normalized rotational transform $\iota/2\pi$ profile, and (c) pressure profile $P_0$.

the higher density gradient at the IDB than that at the edge. In the regime $\langle\beta_{\mathrm{dia}}\rangle > 1\%$, the core gradient increases faster than that before, suggesting the perfect formation of the IDB, although the edge gradient increases monotonically. Important information known from this experimental result, depicted in Fig. 9, is that no saturation in both gradients is seen as an increase in $\langle\beta_{\mathrm{dia}}\rangle$. In other words, the IDB-SDC mode is not limited by the beta so far in the present experimental condition.

From the viewpoint of the stability, it seems that there exists a margin in the IDB-SDC mode, which is confirmed theoretically and experimentally. However, the theoretical equilibrium analysis with the VMEC code is not sufficient, since it cannot deal with the configuration with magnetic islands and/or with the ergodic region in the calculation volume. It also cannot calculate the open region where the magnetic field lines are terminated by the limiter or vessel wall. On the other hand, the HINT2 code,[30] which has recently been developed on the basis of the HINT code, is not limited its calculation volume to perfectly closed surfaces. In that sense, the HINT2 code is suitable for the IDB-SDC plasma analysis in which magnetic field lines are not always perfectly closed. Results of the equilibrium analyses using the HINT2 code are shown in Fig. 10. The calculated pressure profile shown in

Fig. 10(c) reproduces the experimental result. The Shafranov shift calculated by HINT2 agrees well within the error of 15% [compare Figs. 10(c) and 3]. The $\iota/2\pi$ profile in Fig. 10(b) shows a similar trend, as derived with the VMEC code depicted in Fig. 8. The HINT2 prediction suggests almost half of the outer closed region including the superimposed $m/n=1/1$ island is ergodized, as shown in Fig. 10(a). Furthermore, the residual $m/n=2/1$ island due to the intrinsic error field is found to be enhanced. It seems that the 2/1 island is in the ergodic sea. In the HINT code, which is a pure MHD calculation, the island region results in the flat pressure profile, as shown in Fig. 10(c). In the experiment, however, there exists a finite gradient in the region, as seen in Fig. 3, because of the high collisionality there. Although the ergodization in the edge region means the destruction of the confinement volume, the field lines there are so long that they can maintain the finite pressure so far. However, as the edge ergodization enhances more and the confinement volume becomes smaller, it becomes a serious situation. In order to avoid the so-called equilibrium limit, it will be necessary to push the plasma column back by the vertical field control when the beta value becomes higher.

### D. Impurity behavior

In the high-density regime such as an IDB-SDC mode, impurity behavior plays an important role to maintain or enhance the present regime. The impurity accumulation in the core region may bring about the disruptive collapse of the discharge. In the IDB-SDC mode, the impurity behavior and its effect on the energy balance were investigated. Figure 11 shows time evolutions of (c) Fe $K\alpha$ line emission measured with a pulse height analyzer (PHA) for x-ray emission,[31] (d) total radiation power measured with a $2\pi$-bolometer, (e) normalized radial radiation profile measured with a poloidal bolometer array, together with (a) central electron density $n_{e0}$ and (b) central electron temperature $T_{e0}$. Horizontal error bars in Fig. 11(c) represent the time resolution of the PHA, which is 0.2 s.

It is found from Fig. 11(d) that the total radiation increases gradually in the latter half of the discharge. Comparing Figs. 11(d) and 11(e), it seems that the energy is radiated mainly from the core region. The time behavior of the total radiation correlates well with the core radiation depicted in Fig. 11(e), especially from $t\sim 1$ to 1.6 s. The Fe $K\alpha$ line emission shown in Fig. 11(c) also increases with the total and/or core radiation in the latter half of the discharge. It would surely be reasonable to consider that the Fe $K\alpha$ line emission comes from the core region in this temperature range. However, it does not always correlate with the core radiation; i.e., the Fe $K\alpha$ line emission continues to increase while $P_{\mathrm{rad}}$ begins to decreases after $t=1.45$ s. In fact, it seems that Fe $K\alpha$ line emission correlates with $T_{e0}$, rather than $P_{\mathrm{rad}}$. Therefore, it can be considered that the increase of Fe $K\alpha$ line emission may be due to the increase of the central electron temperature, rather than the increase of Fe density itself. In other words, impurity contamination is not as serious in the IDB-SDC mode.

Another qualitative explanation for the increase of the Fe $K\alpha$ line emission may be possible; i.e., it is attributed to the increase of the Fe influx. The high-density plasma in the IDB-SDC mode enhances the sputtering on the vacuum vessel wall, which is made of stainless steel, through the high flux of charge exchange particles. The sputtered carbon released from the plasma-facing components (PFCs), e.g., carbon tiles on the LID head, may also enhance the Fe sputtering on the vacuum vessel wall through the charge exchange process, since the sputtering yield by carbon is much higher than that by hydrogen.

In any case, the core radiation does not terminate the discharge. In view of the fact that the total radiation power is small (about 30% of the total heating power), it is found that the radiation has nothing to do with the termination of the discharge. In fact, the discharge was actually terminated by switching off the NBs in this shot. Sufficient or crucial evidence has not been observed for the impurity accumulation

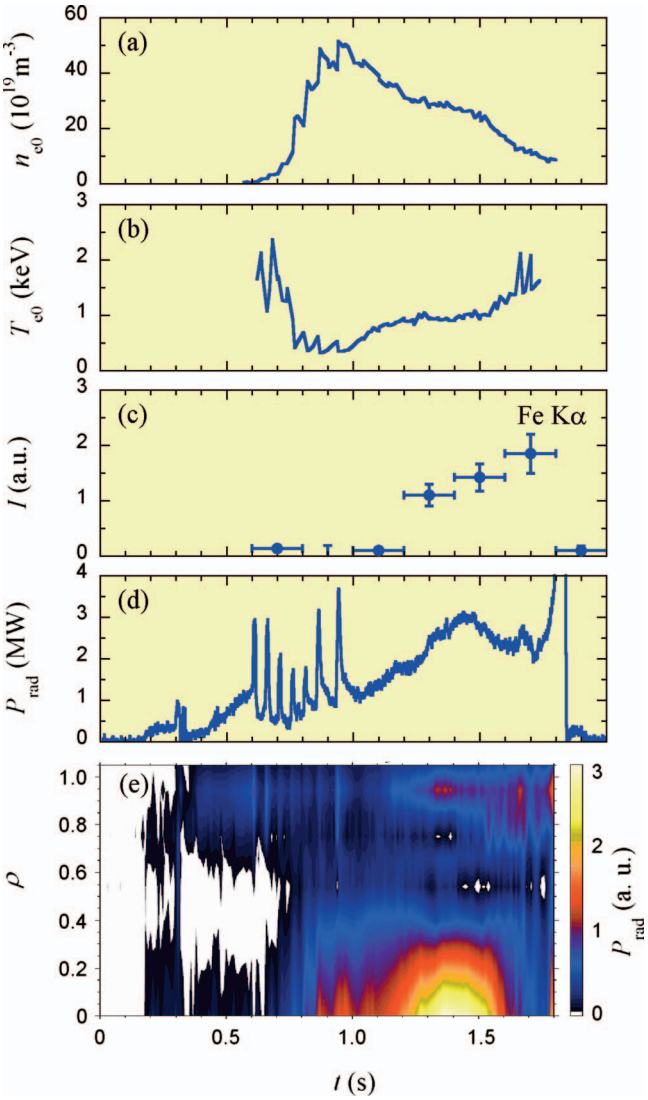


FIG. 11. (Color) Time behavior of (a) central electron density, (b) central electron temperature, (c) Fe $K\alpha$ line emission measured with a pulse height analyzer (PHA) for x-ray emission, (d) total radiation power measured with a $2\pi$-bolometer, and (e) normalized radial radiation profile measured with a bolometer array.

in the core region as yet; therefore, further experimental and theoretical investigations will be necessary to reach the conclusion.

## IV. DISCUSSION

As described in the previous section, the IDB-SDC plasma is an improved mode that has been newly discovered in helical systems. Whether the IDB-SDC mode is to be a principal mode in helical devices is strongly attributed to the possibility to adapt it to the reactor plasma. It is widely accepted that high temperature, i.e., more than 10 keV, is necessary for the self-ignition in fusion reactors. On the other hand, it might be possible to access the self-ignition regime through high density with a relatively low temperature path. From the view point of this novel approach, the IDB-SDC mode has a possibility to be one of the operational modes to obtain a burning plasma. A scheme such as a high-density mode is particularly attractive for helical devices, because operation at the high collisionality regime reduces the helical ripple transport loss that may arise in the conventional approach with a high temperature plasma in the low collisionality regime. In addition, helical devices have no limitation from the plasma current; furthermore, they do not require current drive, which is most effective at low density.

In order to approach the reactor plasma with the IDB-SDC mode, the possibility of the steady-state operation is strongly required. The IDB-SDC mode is essentially a transient phenomenon since it occurs in the density decay or so-called reheat phase.[32] A trial to sustain the IDB-SDC mode for a long time was performed. A continuous pellet injector with small pellet barrels ($\Delta n \sim 1 \times 10^{21}$) was utilized to maintain the pressure profile after the formation of the IDB. By injecting the pellet every 0.13 s, the quasi-steady-state IDB-SDC mode could be successfully maintained for nearly 1 s. In the quasi-steady-state phase, perturbations by the pellets on stored energy and density were ~15%.

For steady-state operation, there is another issue to be solved before advancing further. As described in the previous section, the heat load to the LID is too high to sustain the IDB-SDC mode for a long time. This is due to the essential problem of the LID since its wetted area for the diverted plasma is very small. We cannot avoid this problem insofar as LID is used to achieve the IDB-SDC mode in future. It may be impossible to remove such a high heat load on the LID head, especially in the reactor. However, if the IDB-SDC mode can be achieved without the LID, the issue about the heat handling on PFCs may be solved. Let us consider the essentials to achieve the IDB-SDC mode once again. The necessary conditions for the mode are central fueling (by pellet injection) and strong edge pumping for reduction of edge recycling. To satisfy the second condition, the LID is not always necessary. If edge recycling can be reduced to the LID level by another edge pumping method, it can alternatively be utilized instead of the LID.

A promising result was recently obtained in the HD configuration (without LID). For this trial experiment, exhaustive wall conditioning was carried out before the discharge to reduce recycling, and pellet fueling was also utilized. In Fig. 12, radial profiles of (a) electron density and (b) temperature in the HD configuration (open circles) are presented, together with the LID configuration (closed circles). It can clearly be seen that both profiles between HD and LID are almost the same, except that the central temperature in the HD configuration is slightly low. The global confinement and MHD activities are also similar to each other. Looking at impurity behavior, the HD discharge is better than the LID one; i.e., the Fe $K\alpha$ line emission from the core region can hardly be seen in the HD configuration. Furthermore, radiation from light impurities, e.g., carbon, is also small in the HD configuration. This might be due to the mitigation of the heat load to PFCs. In the present HD configuration without baffle plates (open divertor configuration), however, it is hard to sustain IDB for a long time with continuous pellet injection, which consequently increases the edge density. It has been found that, for the stable IDB-SDC mode, it is essential to keep the electron density at the last closed flux surface below $\sim 5 \times 10^{19}$ m$^{-3}$. In gas puff fueled discharges (edge fueling), the IDB-SDC mode can never be seen. This experimental result has confirmed that the necessary conditions to achieve the IDB are central fueling and strong edge pumping; hence, we are strongly encouraged to suppose that the IDB-SDC mode can be adapted to the reactor in the HD configuration. This conclusion also suggests that the closed configuration is definitely necessary for the HD.

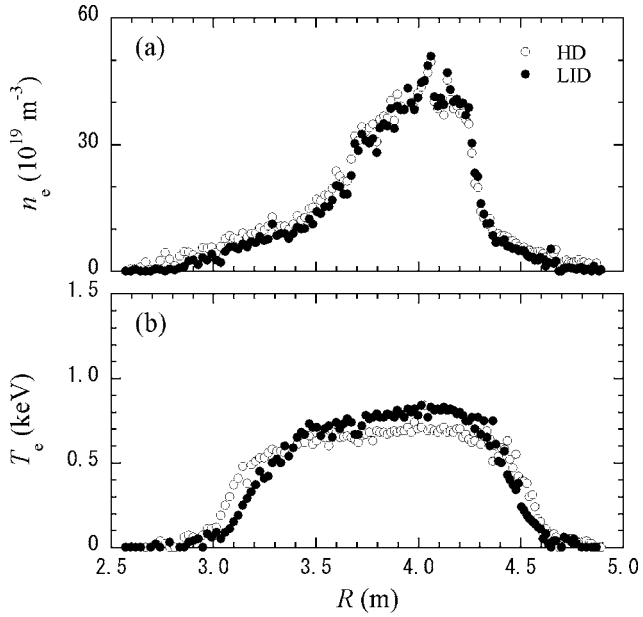


FIG. 12. Radial profiles of (a) electron density and (b) temperature in the HD configuration (open circles), together with the LID configuration (closed circles).

## V. SUMMARY

The superdense core (SDC) mode with central density $\sim 5 \times 10^{20}$ m$^{-3}$ was maintained for ~1 s by the formation of an internal diffusion barrier (IDB) in LHD. The central electron temperature in IDB-SDC plasmas is relatively high: ~0.85 keV. It is considered that low density in the outer region helps to raise the edge temperature gradient there, and

hence the core temperature as well. In order to obtain the IDB-SDC mode, pellet injection (central fueling) and strong edge pumping (low edge recycling) are essential. In the IDB-SDC mode, no serious MHD activity to terminate the discharge has been observed so far. We have never seen the serious impurity accumulation leading the plasma to radiating collapse. Because of the large Shafranov shift due to the high central beta value, the edge magnetic structure is strongly ergodized, which may cause the equilibrium limit.

It is confirmed that the IDB-SDC mode has a possibility to be one of the operational modes to obtain the burning plasma with helical devices.

## ACKNOWLEDGMENTS

The authors would like to thank Dr. J. Harris, Dr. Y. Igitkhanov, and Professor T. Kato for their fruitful discussions and continuous encouragement.

This work is funded by NIFS06ULPP506 and the Grant-Aid for Scientific Research from MEXT of the Japanese government.

[1] F. W. Perkings, D. E. Post, N. A. Uckan *et al.*, Nucl. Fusion **39** 2173 (1999).
[2] F. Wagner, G. Becker, K. Behringer *et al.*, Phys. Rev. Lett. **49**, 1408 (1982).
[3] T. Fujita, T. Hatae, T. Oikawa *et al.*, Nucl. Fusion **38**, 207 (1998).
[4] F. M. Levinton, M. C. Zarnstorff, and S. H. Batha, Phys. Rev. Lett. **75**, 4417 (1995).
[5] E. J. Strait, L. L. Lao, and M. E. Mauel, Phys. Rev. Lett. **75**, 4421 (1995).
[6] M. Wakatani, *Stellarator and Helical Devices* (Oxford University Press, New York, 1998), p. 7.
[7] O. Motojima, H. Yamada, A. Komori *et al.*, Phys. Plasmas **6**, 1843 (1999).
[8] N. Ohyabu, T. Watanabe, H. Ji *et al.*, Nucl. Fusion **34**, 387 (1994).
[9] N. Ohyabu, A. Komori, H. Suzuki *et al.*, J. Nucl. Mater. **266-269**, 302 (1999).
[10] A. Komori, T. Morisaki, S. Masuzaki *et al.*, Fusion Sci. Technol. **46** 167 (2004).
[11] T. Morisaki, S. Masuzaki, A. Komori *et al.*, J. Nucl. Mater. **337-339**, 154 (2005).
[12] T. Morisaki, S. Masuzaki, M. Kobayashi *et al.*, Fusion Sci. Technol. **50**, 216 (2006).
[13] T. Morisaki, K. Narihara, S. Masuzaki *et al.*, J. Nucl. Mater. **313-316**, 548 (2003).
[14] N. Ohyabu, T. Morisaki, S. Masuzaki *et al.*, Phys. Rev. Lett. **97**, 055002 (2006).
[15] R. Sakamoto, H. Yamada, K. Tanaka *et al.*, Nucl. Fusion **41**, 381 (2001).
[16] M. Hugon, B. Ph. van Milligen, P. Smeulders *et al.*, Nucl. Fusion **32**, 33 (1992).
[17] P. H. Rebut, Nucl. Fusion **25**, 1011 (1985).
[18] V. P. Bhatnagar, A. Taroni, J. J. Ellis, J. Jacquinot, and D. F. H. Start, Plasma Phys. Controlled Fusion **31**, 2111 (1989).
[19] B. Balet, D. A. Boyd, D. J. Campbell *et al.*, Nucl. Fusion **30**, 2029 (1990).
[20] H. Renner, W7AS Team, NBI Group, ICF Group, ECRH Group, Plasma Phys. Controlled Fusion **31**, 1579 (1989).
[21] K. McCormick, P. Grigull, R. Burhenn *et al.*, Phys. Rev. Lett. **89**, 015001 (2002).
[22] K. McCormick, P. Grigull, R. Burhenn *et al.*, J. Nucl. Mater. **313-316**, 1131 (2003).
[23] N. Ohyabu, J. S. DeGrassie, and T. E. Evans, J. Nucl. Mater. **145-147**, 844 (1987).
[24] T. E. Evans, J. S. DeGrassie, H. R. Garner *et al.*, J. Nucl. Mater. **162-164**, 636 (1989).
[25] H. Yamada, A. Komori, N. Ohyabu *et al.*, J. Nucl. Mater. **43**, A55 (2001).
[26] U. Stroth, M. Murakami, R. A. Dory *et al.*, Nucl. Fusion **36**, 1063 (1996).
[27] H. Yamada, S. Murakami, and K. Yamazaki, Nucl. Fusion **43**, 749 (2003).
[28] S. P. Hirshman, W. I. van Rij, and P. Merkel, Comput. Phys. Commun. **43**, 143 (1986).
[29] C. Nuehrenberg, Phys. Plasmas **6**, 137 (1999).
[30] Y. Suzuki, N. Nakajima, K. Watanabe, Y. Nakamura, and T. Hayashi, Nucl. Fusion **46**, L19 (2006).
[31] S. Muto, S. Morita, S. Kubo, T. Shimozuma, H. Idei, and Y. Yoshimura, Rev. Sci. Instrum. **74**, 1993 (2003).
[32] S. Morita, H. Yamada, H. Iguchi *et al.*, *Proceedings of the 14th International Conference on Plasma Physics and Controlled Nuclear Fusion Research*, Wuerzburg, 1992 (IAEA, Vienna, 1993), Vol. 2, p. 515.